Data Article

# Second-life lithium-ion battery aging dataset based on grid storage cycling

Kevin Moy [a,1], Muhammad Aadil Khan [a,1], Simone Fasolato [a,b], Gabriele Pozzato [a], Anirudh Allam [a], Simona Onori [a,*]

[a] Department of Energy Science and Engineering, Stanford University, 367 Panama St, Stanford, CA 94305, United States
[b] Department of Electrical, Computer and Biomedical Engineering University of Pavia, 27100 Pavia, Italy

## ARTICLE INFO

## ABSTRACT

This paper describes an experimental dataset of used lithium-ion battery cells cycled on grid storage synthetic duty cycles to study their feasibility for second-life applications. Data were collected at the Stanford Energy Control Laboratory at Stanford University, CA, USA. The ten INR21700-M50T battery cells with graphite/silicon anode and Nickel–Manganese–Cobalt (NMC) cathode had been previously tested over a period of 23 months according to the Urban Dynamometer Driving Schedule (UDDS) discharge driving profile. In this paper, six out of these ten cells are tested for a period of 24 months. The aging campaign is a combination of calendar aging and cycling. The cycling portion is designed to replicate real-world usage patterns based on synthetic duty cycles for residential and commercial grid energy storage systems (ESS). Battery cycling alternates between 20 °C and 35 °C to simulate seasonal temperature variations encountered in grid applications. The calendar aging, on the other hand, occurs at room temperature. Periodic assessments of battery degradation during second-life testing are accomplished via Reference Performance Tests for second-life (RPT S) comprising of a combined capacity and pulse power test, and Electrochemical Impedance Spectroscopy (EIS) at three state-of-charge (SOC) values. The data

* Corresponding author.
  E-mail address: sonori@stanford.edu (S. Onori).
[1] These authors contributed equally.

set captures the combined effects of cycling-induced stress and long-term storage.

## Specifications Table

| | |
|---|---|
| Subject | Electrical and Electronic Engineering |
| Specific subject area | Second-life grid-storage dispatch and diagnostic tests of lithium-ion batteries |
| Type of data | Table |
| Data collection | Hardware:<br><br>• Arbin Instruments LBT21024 and Arbin measurement system<br>• Amerex IC500R thermal chamber<br>• Gamry EIS 1010E<br>• T-type thermocouple sensor, Omega<br><br>Software:<br><br>• MITS Pro software and Data Watcher |
| Data source location | Institution: Stanford Energy Control Lab, Energy Science and Engineering Department, Doerr School of Sustainability, Stanford University<br>City, State: Stanford, California<br>Country: United States of America<br>Latitude and longitude for collected samples/data:<br>(37.426666918636386, −122.17397631867011) |
| Data accessibility | Repository name: Open Science Framework<br>Data identification number: DOI 10.17605/OSF.IO/8JNR5<br>Direct URL to data: https://osf.io/8jnr5/ |
| Related research article | None |

## 1. Value of the Data

- This dataset is based on six lithium-ion battery (LIB) cells that had been previously cycled according to the Urban Dynamometer Driving Schedule (UDDS) profile for a period of 23 months and degraded down to 90 % of their nominal capacity [1]. In this work, grid-storage synthetic duty cycles [2] are used to cycle these cells to understand their performance for a second-life application. These cycles are designed to represent peak shaving operation for two energy storage systems (ESSs): one residential ESS, and one commercial ESS. The aging campaign alternates between 20 °C and 35 °C to replicate the seasonal changes in temperature experienced by LIBs in the field.
- Diagnostic tests, such as capacity test with pulses and Electrochemical Impedance Spectroscopy (EIS), were performed at 25 °C to obtain battery aging data comparable to the aging data obtained from first-life experiments.
- To the best of the authors' knowledge, this dataset is the first of its kind to provide battery aging data from application-specific operation that is expected to be encountered by second-life batteries. It provides a quantitative overview of used batteries in a grid-storage setting, and it can also enable the development of dedicated state-of-health (SOH) models and algorithms for second-life operations.

## 2. Background

Batteries retired from electric vehicles (EVs) present promising opportunities for use in stationary applications [3], such as commercial or residential settings. However, current research on

second-life batteries is hindered by lack of realistic datasets that capture their performance and behavior [4]. To overcome this, in this paper, we utilize synthetic duty cycles that represent ESS operation in residential and commercial settings [5] to generate an aging dataset for second-life batteries' assessment.

## 3. Data Description

The dataset is composed of cycling data from grid storage synthetic duty cycle profiles and Reference Performance Test (RPT S) data for six INR21700-M50T NMC cells over a period of 24 months. These cells are a subset of the ten cells originally cycled using an EV driving profile in [1]. Technical specifications of the cells are summarized in Table 1.

The synthetic duty cycles developed in [2] are shown in Fig. 1. The residential synthetic duty cycle (Fig. 1(a)) represents peak shaving for a residential single-family home, while the commercial synthetic duty cycle (Fig. 1(b)) represents peak shaving for an office building [5,8]. In both cases, each complete duty cycle spans 48 h (2 days) and includes both charging and discharging phases. The current and power convention applied in this paper defines charging as negative and discharging as positive.

The six cells used in this work are listed in Table 2. The study in [1] used different charging C-rates for different cells resulting in a large variation in the number of cycles completed and the remaining capacity at the end of first-life. Cells V4 and W8 were cycled with a low

**Table 1**
Technical specifications of INR21700-M50T cell [6].

| | |
|---|---|
| Manufacturer | LG Chem |
| Model | INR21700-M50T |
| Positive electrode | LiNiMnCoO2 |
| Negative electrode | Graphite and silicon [7] |
| Size (diameter x length) | 21.44 mm × 70.80 mm |
| Weight | 69.25 g |
| Nominal capacity ($Q_{nom}$) | 4.85 Ah |
| Nominal voltage ($V_{nom}$) | 3.63 V |
| Charge cutoff voltage ($V_{chg,cutoff}$) | 4.2 V |
| Discharge cutoff voltage ($V_{dch,cutoff}$) | 2.5 V |
| Cutoff current ($I_{cutoff}$) | 50 mA |
| Standard charging current ($I_{chg,st}$) | 1.455 A |
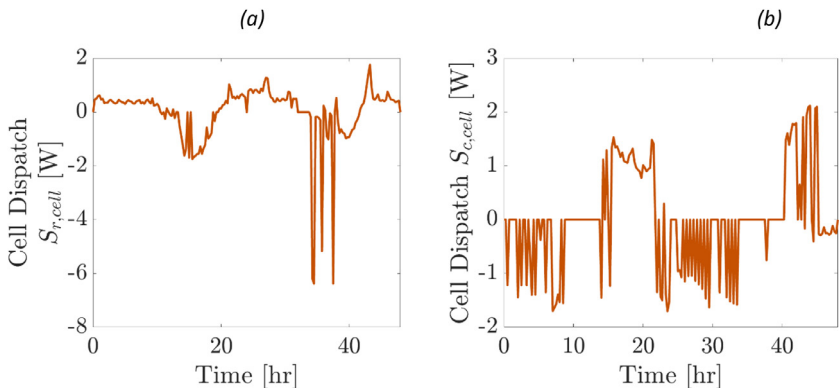


**Fig. 1.** Grid storage synthetic duty cycles used in this paper to cycle the cells. (a) Residential ESS synthetic duty cycle. (b) Commercial ESS synthetic duty cycle.

**Table 2**

Six cells with charging C-rate in the first-life, number of cycles completed, and capacity at the end of first-life [1]. Cells are divided randomly to cycle with a residential or commercial synthetic duty cycle.

| Cell Name | Charge C-rate in first-life [1/h] | Number of cycles completed in first-life | Capacity at end of first-life [Ah] | Synthetic duty cycles |
|---|---|---|---|---|
| V4 | C/4 | 244 | 4.6024 | Residential |
| W8 | C/2 | 347 | 4.4568 | Commercial |
| W9 | 1C | 341 | 4.4636 | Residential |
| V5 | 1C | 29 | 4.7055 | Commercial |
| W10 | 3C | 350 | 4.4591 | Residential |
| G1 | 3C | 212 | 4.6000 | Commercial |

C-rate of C/4 and C/2, respectively. Cells W9 and V5 were both cycled at 1C, and cells W10 and G1 were both cycled at 3C. For this study, these cells were evenly and randomly split between the residential and commercial synthetic duty cycles, and began cycling on October 28, 2022. As shown in Fig. 2, the aging campaign begins with RPT S-1 at 25 °C consisting of a capacity test with pulses at three different voltage values. Afterwards, the cells undergo cycling at 35 °C using both commercial and residential synthetic duty cycles followed by the RPT S-2 at 25 °C. The next cycling batch uses the same synthetic duty cycles, but at 20 °C. In this way, cycling batches alternate between 20 °C and 35 °C to replicate the varying temperature conditions in a grid setting. It should be noted that at RPT S-5, Electrochemical Impedance Spectroscopy (EIS) was also conducted, and it remained a part of the RPT S for the remainder of the aging campaign. Lastly, the cells also undergo calendar aging during periods when the experiments were stopped. The first calendar aging occurs just before the 11th RPT for a period of about 19 days. The data shared is until October 6th, 2024; however, further experiments are ongoing, and the data repository will be updated as new data is collected. Details of the aging campaign are given in Table 3.

A cycling batch follows a sequence of 7 steps as listed in Table 4. Before starting Step 1, the cells are kept idle in the thermal chamber for a temperature soak for at least 1-h. Afterwards, a constant current (CC) charge is performed at the standard charging current $I_{chg,st} = $ 1.455 A. Once the battery voltage reaches $V_{chg,cutoff} = 4.2$ V, a constant voltage (CV) phase starts (Step 2) until the current reaches below $I_{cutoff} = 50$ mA, followed by a 1-hour rest (Step 3). Next, Step 4 (CC discharge at 1C for 30 min) is designed to bring the battery to a mid-range SOC, approximately 42 %, followed by another 1-h rest (Step 5). Step 6 cycles the battery using the corresponding synthetic duty cycle five times, totalling 10 days of cycling. In this step, the inputs to the battery cycler for all six cells are power profiles as shown in Fig. 1. Figs. 3 and 4 show examples of current, voltage, and power for one batch of residential and commercial synthetic duty cycles for cells W10 and W8, respectively. Finally, the batch concludes with a 1-h rest (Step 7). As indicated in Table 3, from batch 4 to 15, all the cycling is performed with two contiguous batches consisting of 5 cycles each resulting in a total of 20 days of cycling. These batches are represented by Batch #-1 and Batch #-2.

The RPT S are run periodically between batches at 25 °C. Each RPT S consists of a capacity test with pulses. Starting from the 5th RPT S, EIS test is also conducted, as mentioned previously.

The capacity test with pulses is summarized in Table 5. After bringing the cell to $V_{chg,cutoff}$ representing 100 % SOC, the test discharges the cell at C/20, and applies pulses at 4.00 V, 3.63 V, and 3.26 V. These voltages represent the upper voltage bound experienced during cycling, the nominal voltage, and the lower voltage bound experienced during cycling, respectively. Each pulse sequence consists of an 8 s C/2 discharge, followed by a 10 s rest, followed by an 8 s C/2 charge. After discharging to $V_{dch,cutoff} = 2.5$ V, the cell is charged at $I_{chg,st}$ until the cell reaches $V_{nom}$, to ensure that the cell does not remain at a low voltage and induce any unnecessary degradation on the cell. An example of this protocol is shown in Fig. 5 for cell W9 at RPT S-8. All protocols include exit conditions dependent on the cell voltage $V_{cell}$ and current $I_{cell}$, respectively. For all protocols, the C-rate used for each cell is determined from the capacity value obtained
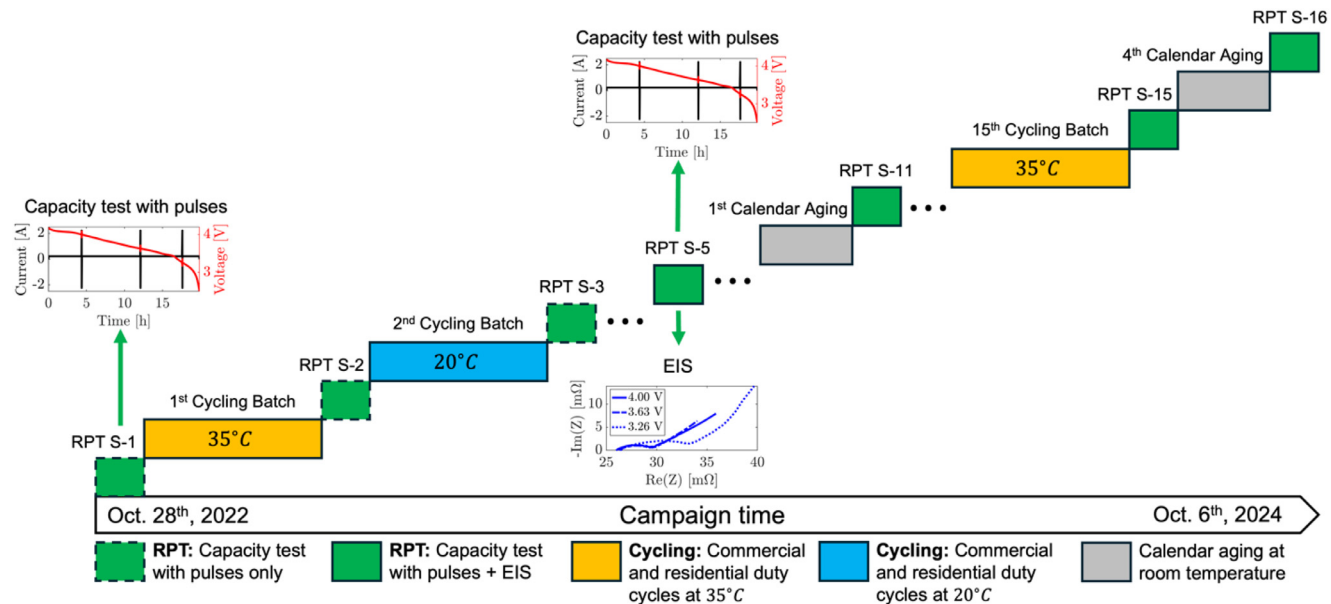
**Fig. 2.** Overview of the aging campaign over a period of 24 months. Dashed green box represents RPT S consisting of capacity test with pulses only and solid green box represents RPT S with capacity test with pulses and EIS. For cells being cycled with both residential and commercial synthetic duty cycles, the cycling temperature alternates between 35 °C and 20 °C throughout the campaign. Cells also undergo calendar aging at room temperature. (For interpretation of the references to color in this figure legend, the reader is referred to the web version of this article.)

**Table 3**

Summary of sequence of protocols (cycling and calendar) used for second-life aging experiments. The temperature is configured as the thermal chamber setpoint. Note: When number of cycles are not specified in Notes, it means each batch consists of 5 cycles e.g., Batch 4-1 has 5 cycles and Batch 4-2 has 5 cycles.

| Protocol Name | Temperature [C] | Start date | Notes |
|---|---|---|---|
| Batch 1 | 35 | 2022-10-28 | 8 cycles |
| RPT S-1 | 25 | 2022-11-14 | No EIS |
| Batch 2 | 20 | 2022-12-06 | 5 cycles |
| RPT S-2 | 20 | 2022-12-16 | Chamber setpoint incorrectly configured |
| Batch 3 | 35 | 2022-12-31 | ~9 cycles |
| RPT S-3 | 25 | 2023-01-16 | No EIS |
| Batch 4-1 | 20 | 2023-02-07 | |
| Batch 4-2 | 20 | 2023-02-17 | |
| RPT S-4 | 25 | 2023-02-28 | No EIS |
| Batch 5-1 | 35 | 2023-03-02 | |
| Batch 5-2 | 35 | 2023-03-12 | |
| RPT S-5 | 25 | 2023-03-22 | |
| Batch 6-1 | 20 | 2023-03-29 | |
| Batch 6-2 | 20 | 2023-04-09 | |
| RPT S-6 | 25 | 2023-04-21 | |
| Batch 7-1 | 35 | 2023-04-27 | |
| Batch 7-2 | 35 | 2023-05-08 | |
| RPT S-7 | 25 | 2023-05-18 | |
| Batch 8-1 | 20 | 2023-05-26 | |
| Batch 8-2 | 20 | 2023-06-06 | |
| RPT S-8 | 25 | 2023-06-22 | |
| Batch 9-1 | 35 | 2023-07-22 | |
| Batch 9-2 | 35 | 2023-08-02 | |
| RPT S-9 | 25 | 2023-08-14 | |
| Batch 10-1 | 20 | 2023-08-23 | |
| Batch 10-2 | 20 | 2023-09-03 | |
| RPT S-10 | 25 | 2023-09-14 | |
| Batch 11-1 | 35 | 2023-09-20 | |
| Batch 11-2 | 35 | 2023-10-01 | |
| Calendar 1 | Room temperature | 2024-10-11 | Storage voltage: V4 at 3.653 V, W8 at 3.6920 V, W9 at 3.6910 V, V5 at 3.6760 V, W10 at 3.7010 V, and G1 at 3.6640 V |
| RPT S-11 | 25 | 2023-10-30 | |
| Batch 12-1 | 20 | 2023-11-06 | |
| Batch 12-2 | 20 | 2023-11-17 | |
| RPT S-12 | 25 | 2023-11-28 | |
| Calendar 2 | Room temperature | 2024-12-05 | Storage voltage: V4 at 3.3130 V, W8 at 3.3240 V, W9 at 3.3170 V, V5 at 3.3050 V, W10 at 3.3030 V, and G1 at 3.3050 V |
| Batch 13-1 | 35 | 2023-12-18 | |
| Batch 13-2 | 35 | 2023-12-29 | |
| RPT S-13 | 25 | 2024-01-08 | |
| Batch 14-1 | 20 | 2024-01-13 | |
| Batch 14-2 | 20 | 2024-01-23 | |
| RPT S-14 | 25 | 2024-02-03 | |
| Calendar 3 | Room temperature | 2024-02-07 | Storage voltage: V4 at 3.3063 V, W8 at 3.3241 V, W9 at 3.3124 V, V5 at 3.3077 V, W10 at 3.2975 V, and G1 at 3.3005 V |
| Batch 15-1 | 35 | 2024-03-18 | |
| Batch 15-2 | 35 | 2024-03-30 | |
| RPT S-15 | 25 | 2024-04-09 | |
| Calendar 4 | Room temperature | 2024-04-09 | Storage voltage: V4 at 3.3340 V, W8 at 3.3563 V, W9 at 3.3410 V, V5 at 3.3454 V, W10 at 3.3420 V, and G1 at 3.3456 V |
| RPT 16 | 25 | 2024-08-01/ 2024-10-05 | RPT S for V4, W9, W10 performed on 2024-08-01; RPT S for G1, W8, V5 performed on 2024-10-05 |
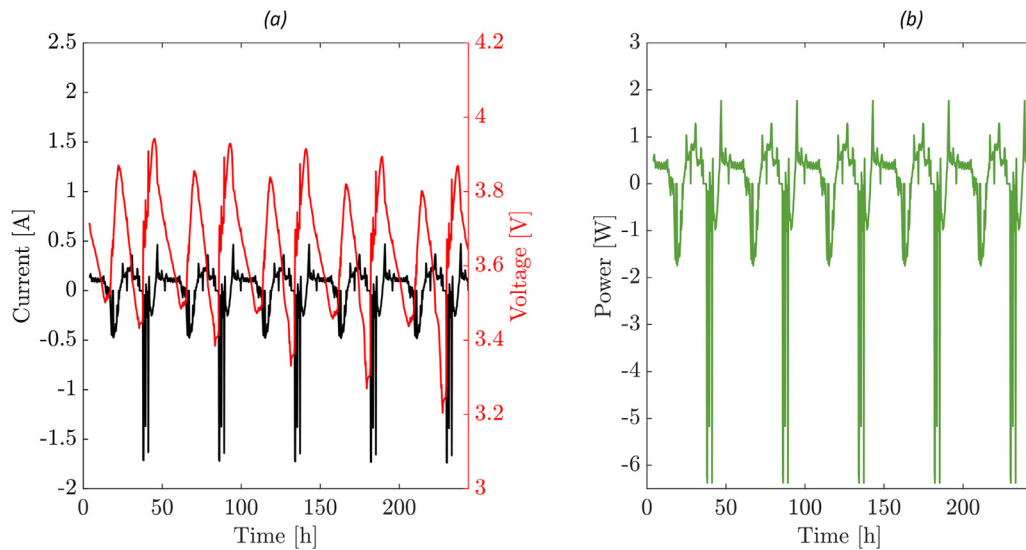
**Fig. 3.** Example of batch cycling data with the residential synthetic duty cycle from cell W10 showing (a) voltage and current, and (b) power.
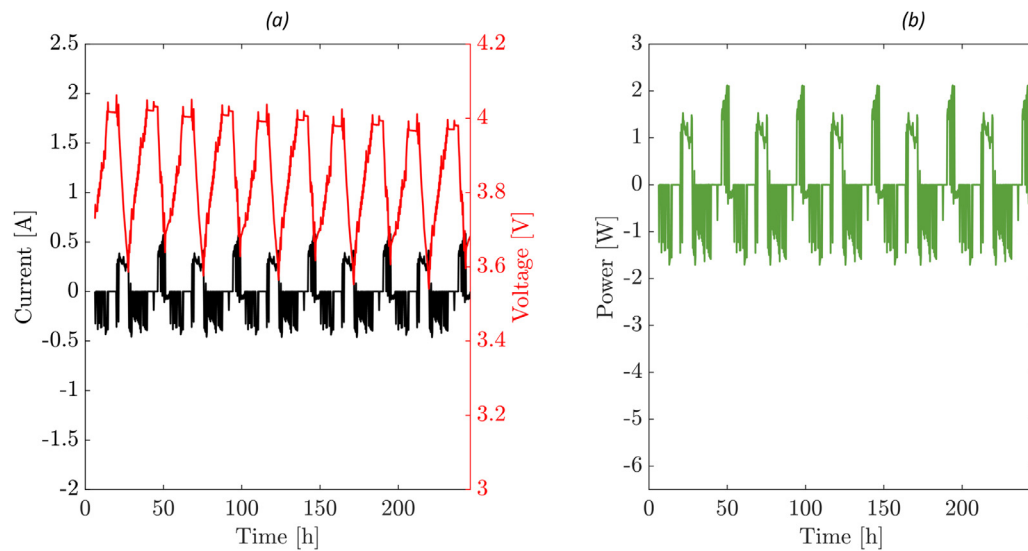
**Fig. 4.** Example of batch cycling data with the commercial synthetic duty cycle from cell W8 showing (a) voltage and current, and (b) power.

**Table 4**

Testing protocol for one batch of second-life synthetic duty cycling. Each cell is CC/CV charged to the upper cutoff voltage $V_{chg,cutoff}$ with CV threshold $I_{cutoff}$ as defined in Table 1. Each cell is then cycled with their respective synthetic duty protocols 5 times, for a total of 10 days of cycling (2 days per each synthetic duty cycle).

| Step | Action | Exit condition | Notes |
|------|--------|----------------|-------|
| 1 | CC charge at $I_{chg,st}$ | $V_{cell} \geq V_{chg,cutoff}$ | Establish 100 % SOC |
| 2 | CV hold at $V_{chg,cutoff}$ | $I_{cell} \leq I_{cutoff}$ | |
| 3 | Rest | 1 h | |
| 4 | CC discharge at 1C | 30 min | Discharge to mid-range SOC |
| 5 | Rest | 1 h | |
| 6 | Power profile cycling | 10 days | 5x synthetic duty cycles (2 days/cycle) |
| 7 | Rest | 1 h (at least) | |

**Table 5**

Sequence of steps in Capacity test with pulses protocol for the RPT S in the aging campaign.

| Action | Exit condition | Notes |
|--------|----------------|-------|
| CC charge at $I_{chg,st}$ | $V_{cell} \geq V_{chg,cutoff}$ | Establish 100 % SOC |
| CV hold at $V_{chg,cutoff}$ | $I_{cell} \leq I_{cutoff}$ | |
| Rest | 1 h | |
| CC discharge at C/20 | $V_{cell} \leq 4.00$ V | ≈ 79.3% SOC for fresh cell |
| Discharge pulse at C/2 | 8 s | |
| Rest | 10 s | |
| Charge pulse at C/2 | 8 s | |
| CC discharge at C/20 | $V_{cell} \leq 3.63$ V | ≈ 44% SOC for fresh cell |
| Discharge pulse at C/2 | 8 s | |
| Rest | 10 s | |
| Charge pulse at C/2 | 8 s | |
| CC discharge at C/20 | $V_{cell} \leq 3.26$ V | ≈ 13% SOC for fresh cell |
| Discharge pulse at C/2 | 8 s | |
| Rest | 10 s | |
| Charge pulse at C/2 | 8 s | |
| CC discharge at C/20 | $V_{cell} \leq V_{dch,cutoff}$ | Lower operating limit of cell |
| Rest | 1 h | |
| CC charge at $I_{chg,st}$ | $V_{cell} \leq V_{nom}$ | Rest to mild voltage |
| Rest | 1 h (at least) | |
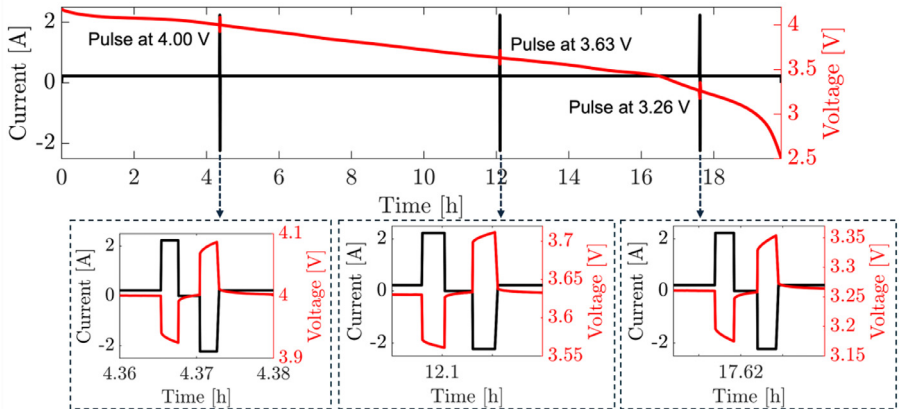


**Fig. 5.** Example of capacity test with pulses for cell W9. Top: Current (black) profile at C/20 constant current discharge with three pulses occurring at 4.00 V, 3.63 V, and 3.26 V at a C-rate of C/2. The corresponding change in voltage (red) is overplotted. Bottom: Pulse regions of the profile are magnified and shown for all the three pulses. (For interpretation of the references to color in this figure legend, the reader is referred to the web version of this article.)
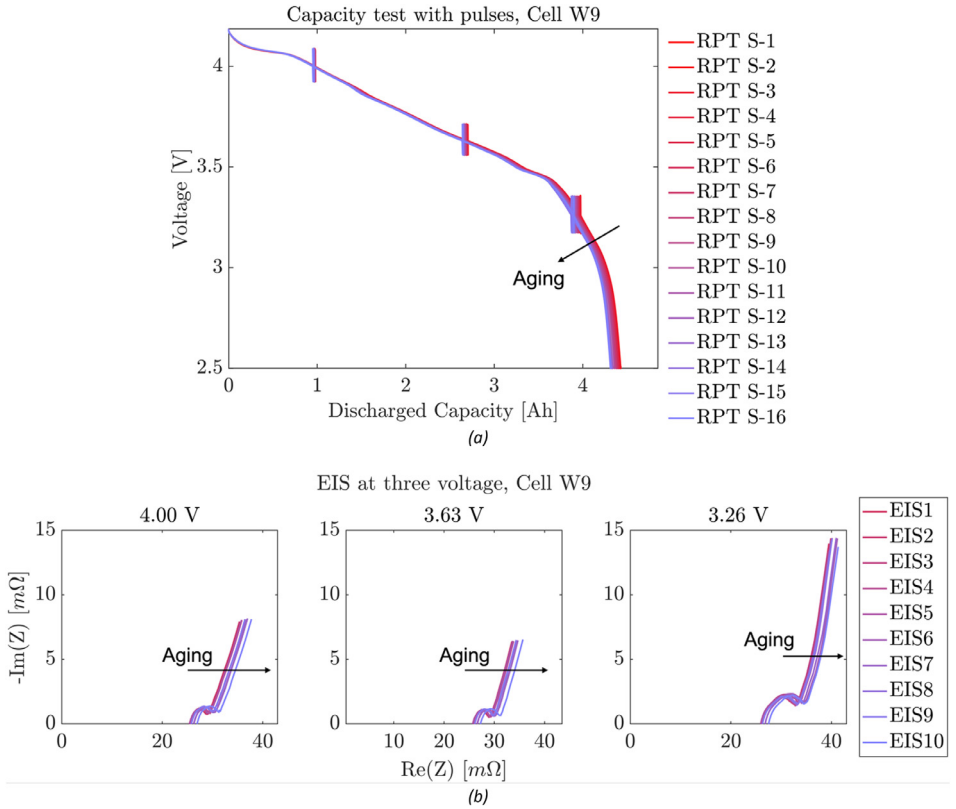
**Fig. 6.** Battery aging for cell W9. (a) Voltage from the C/20 capacity test with pulses shifts inward when plotted against the cell discharge capacity. (b) EIS curves at 4.00 V, 3.63 V, and 3.26 V move towards the right as the battery ages.

from the previous RPT S; batch 1 used the cell capacity measured at the end of first-life as given in Table 2.

As the cells go through the aging campaign, the available capacity of the cell decreases resulting in an inward shift of the voltage curve as shown in Fig. 6(a) for cell W9. The pulses at 3.63 V and 3.26 V also shift towards the left with aging.

EIS is performed to assess the battery impedance in the range of 0.01 Hz and 10 kHz and it is conducted at the same voltage at which the pulses are scheduled in the capacity test with pulses (4.00 V, 3.63 V, and 3.26 V). Fig. 6(b) shows the Nyquist plot at three different voltages for cell W9. With aging, the EIS curves shift to the right. Furthermore, EIS curves at 3.26 V are larger than the EIS curves at the other two voltages with the low frequency impedance value reaching 40 mΩ on the real axis.

Discharge capacity, $Q_{dis}$, for each cell is calculated from the capacity test with pulses by

$$Q_{dis} = \frac{\frac{1}{3600} \int I_{cell}(t)dt}{Q_{nom}} \times 100 \ [\%] \tag{1}$$

where 3600 is the seconds to hours conversion factor, $I_{cell}(t)$ is the C/20 constant current, and $Q_{nom}$ is the fresh cell nominal capacity. Discharged capacity trends for each cell are shown in Fig. 7, as a function of Ampere-hour throughput from second-life cycling. These are accumulated Ampere-hours only during the second-life cycling of the cells. All the cells undergo approximately 1000 to 1200 Ampere-hour throughput with cells under residential synthetic duty cycles (V4, W9, W10) accumulating higher Ampere-hour throughput. The capacity data points
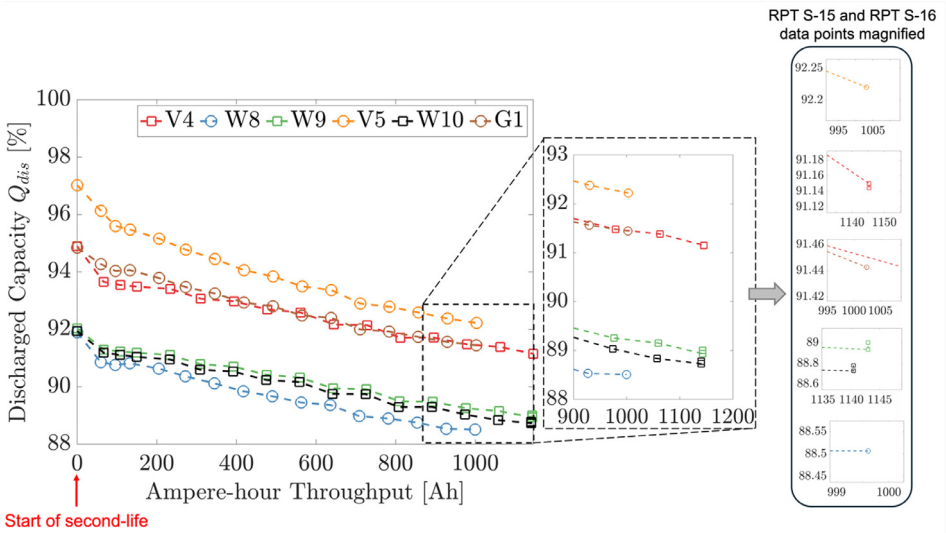
**Fig. 7.** Discharge capacity of six cells as a function of Ampere-hour throughput, calculated using Eq. (1). The x-axis begins at zero, representing Ampere-hours accumulated solely during second-life cycling. Capacity changes due to calendar aging during storage are highlighted on the right by magnifying values from RPT S-15 and RPT S-16. Cells V4, W9, and W10 show minimal calendar aging.
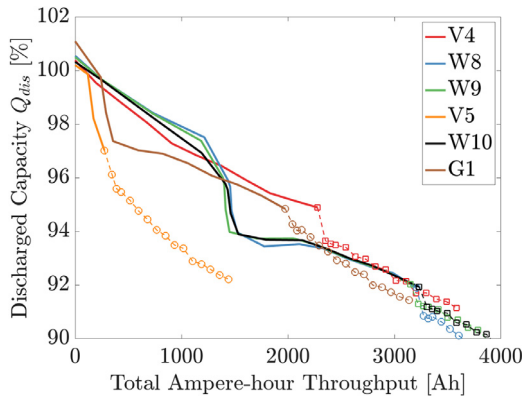


**Fig. 8.** Combined first-life (solid line) and second-life (circle-dashed) discharge capacity of six cells as a function of total Ampere-hour throughput. The x-axis represents the cumulative Ampere-hour throughput across both first and second life phases. Cell V5 has the lowest accumulated Ampere-hours, while cells W9 and W10 show the highest.

for RPT S-15 and RPT S-16 are overplotted (due to no cycling in between them); despite being in storage for 3–5 months, the six cells undergo little to no calendar aging.

Fig. 8 shows the combined first-life and second-life discharged capacity variation of the cells against total Ampere-hour throughput obtained by combining first-life and second-life accumulated Ampere-hour throughput. Cells W9 and W10 accumulate the highest Ampere-hours while cell V5 accumulates the fewest.

In Fig. 9, the bar chart shows a comparison between the initial and final discharge capacity of the cells during second-life. Cells G1, V4, and V5, which started off being higher than the average initial capacity (red-dashed line), remained above the average final capacity (blue-dashed line) at the end of the campaign. Similarly, the remaining three cells started below the average initial
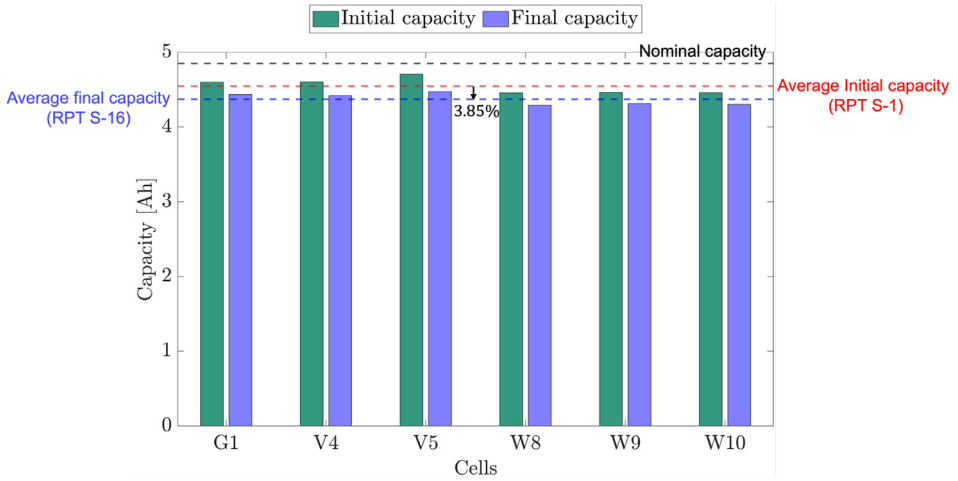
**Fig. 9.** Bar plot of initial and final discharge capacity for all the cells during second-life. Initial capacity corresponds to capacity obtained from RPT S-1 and final capacity corresponds to capacity obtained from RPT S-16. The average decrease in capacity is 3.85 %.
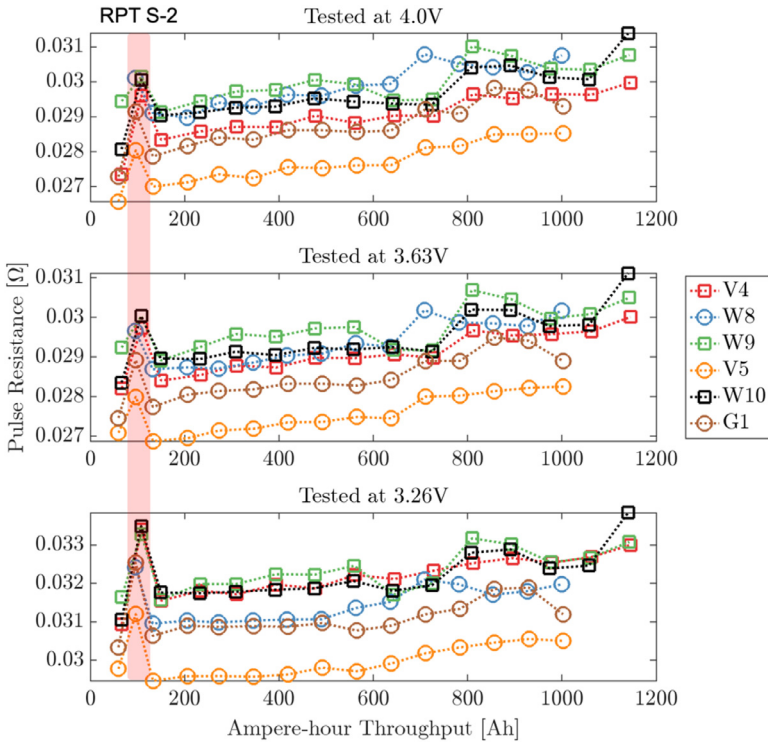


**Fig. 10.** Pulse resistance computed from capacity tests with pulses as a function of Ampere-hour throughput. Cells cycled with residential synthetic duty cycles are shown with square markers, while cells cycled with commercial synthetic duty cycles are shown with circular markers. Note that the second datapoint for each cell corresponds to RPT S-2 in Table 5, which was collected at 20 °C. All other remaining RPT S were conducted at 25 °C.
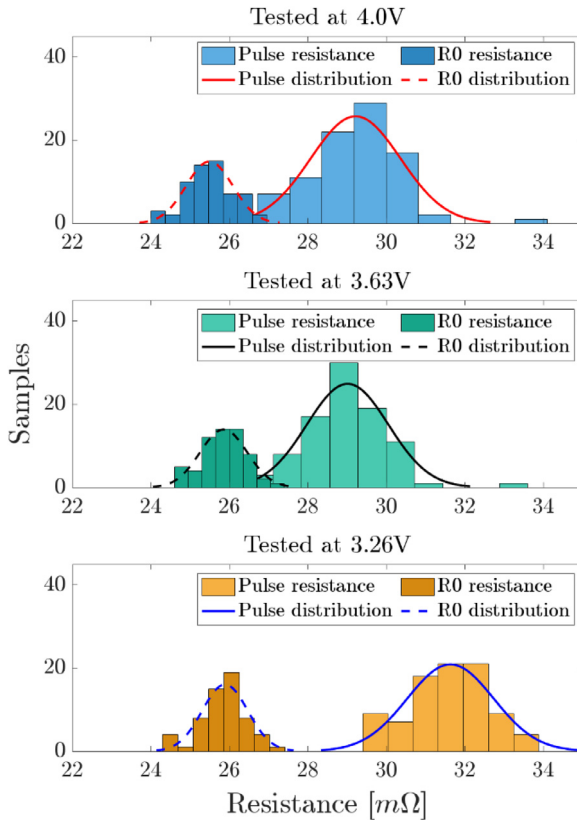
**Fig. 11.** Comparison of distribution of pulse resistances and high-frequency resistances ($R_0$) for all 6 cells at three different voltages. All distributions fit a normal distribution, and high-frequency resistances have similar distributions at all three voltages. On the other hand, pulse resistances have distributions with higher resistance values such as the pulse resistance distribution at 3.26 V.

capacity and ended below the average final capacity. Overall, on average, the capacity of the cells degraded by 3.85 %.

The cell ohmic resistance obtained from pulses at 4.00 V, 3.63 V, and 3.26 V as a function of Ampere-hour throughput is shown in Fig. 10. For RPT S-2, the test was performed at 20 °C resulting in a jump in the resistance for all three voltages. With aging, pulse resistances show an increasing trend with cell W10 reaching the maximum resistance value at the end of cycling among all cells. Fig. 11 illustrates the comparison between the distribution of pulse resistances from capacity test with pulses, and high-frequency resistances ($R_0$) obtained from EIS data for all cells at the same three voltage levels. $R_0$ distributions tend to center around approximately 25.5–26 mΩ at all three voltages; however, the pulse resistances have a wider spread and center around 29–30 mΩ for 4.00 V and 3.63 V. At the low voltage of 3.26 V, the pulse resistance distribution centers around 32 mΩ indicating higher battery resistance at low SOC.

## 3.1. Dataset structure

The dataset consists of raw (.xlsx) data saved in Excel spreadsheets, which can be used to extract diagnostic and cycling data directly.
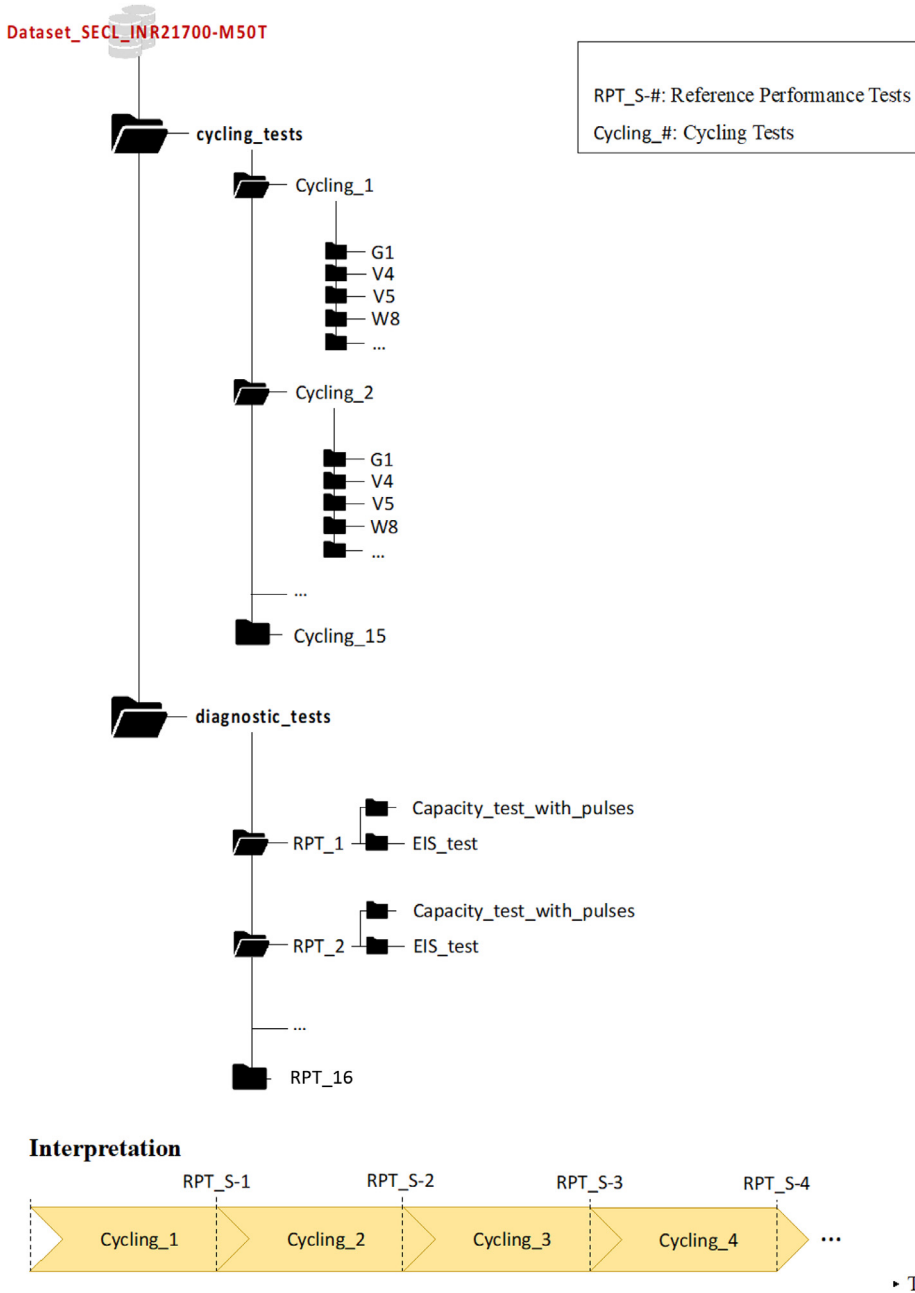
**Fig. 12.** Dataset folder structure.

**Fig. 13.** Equipment available at the Stanford Energy Control Lab (https://onorilab.stanford.edu).
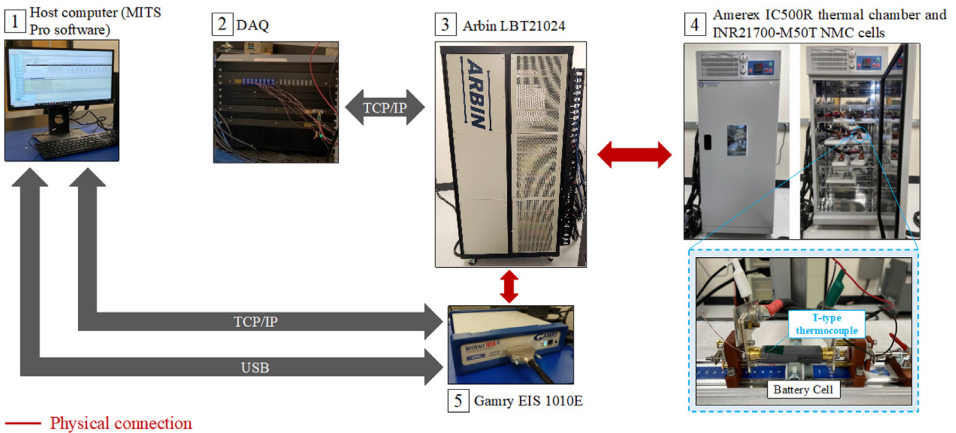
The dataset folder, available online (as specified in the "Data accessibility" field), is structured as in Fig. 12. The parent folder Dataset_SECL_INR21700-M50T has two sub-directories: cycling_tests and diagnostic_tests.

The folder cycling_tests contains the aging cycling data for all the cells. Cycling data are divided into the folders Cycling_# (with # = 1...,...,15). Each folder Cycling_# collects both raw data, divided by cell (i.e., G1, V4, etc.), and processed data, inside _processed_mat. Raw cycling tests are composed of several .xlsx files, that must be merged for the analysis. The .mat files are obtained after merging raw .xlsx files and are available to the user. Inside the folder _processed_mat, the Matlab script data_analysis.m is provided to plot voltage and current profiles.

As shown in Fig. 11, between two cycling folders, RPT S are performed and collected into diagnostic_tests. Raw data for each RPT S are divided into folders named RPT_S-# (with # = 1...,...,16). For example, RPT S-1 in Table 3 corresponds to RPT_S-1. Each folder RPT_S-# contains capacity test with pulses and EIS tests inside the subfolders Capacity_test_with_pulses and EIS_test, respectively.

## 4. Experimental Design, Materials and Methods

Cycling and diagnostic experiments were performed with the equipment available at the Stanford Energy Control Lab (Fig. 12), identical to the setup in [1]. Both cycling and diagnostic tests were designed with the MITS Pro software which allows the design of protocols through a sequence of steps to be followed to perform an experiment. The DAQ is interfaced with Arbin LBT21024, which generates and inputs the desired current profile to the six INR21700-M50T NMC cells tested and measures the output voltage. Each cell is tested inside the Amerex IC500R thermal chamber and instrumented with a T-type thermocouple to measure the surface temperature in the center location. The Gamry EIS 1010E is connected to the Arbin LBT21024 and MITS Pro (via USB link) and used to perform EIS tests at different voltages, namely: 4.00 V, 3.63 V, and 3.26 V.

Each test is exported in .xlsx files containing raw data structures that can be conveniently converted into .mat files (Fig. 13).

## Limitations

None.

## Ethics Statement

Hereby, we Simona Onori, Kevin Moy, Muhammad Aadil Khan, Simone Fasolato, Gabriele Pozzato, and Anirudh Allam assure that for the manuscript *Second-life lithium-ion battery aging dataset based on grid storage cycling* the following is fulfilled:

- This material is the authors' own original work, which has not been previously published elsewhere.
- The paper is not currently being considered for publication elsewhere.
- The paper reflects the authors' own research and analysis in a truthful and complete manner.
- The results are appropriately placed in the context of prior and existing research.
- All sources used are properly disclosed. Literal copying of text is indicated as such by using quotation marks and giving proper reference.
- All authors have been personally and actively involved in substantial work leading to the paper and will take public responsibility for its content.

## CRediT Author Statement

**Kevin Moy:** Methodology, Software, Formal analysis, Investigation, Data Curation, Writing – Original Draft, Visualization. **Muhammad Aadil Khan:** Software, Formal analysis, Investigation, Data Curation, Writing – Original Draft, Visualization, Writing – Review & Editing. **Simone Fasolato:** Methodology, Writing – Review & Editing. **Gabriele Pozzato:** Methodology. **Anirudh Allam:** Methodology. **Simona Onori:** Conceptualization, Methodology, Writing – Review & Editing, Supervision, Funding acquisition.

## Data Availability

Second-life lithium-ion battery aging dataset based on grid storage cycling (Original data) (Open Science Framework).

## Acknowledgments

## Declaration of Competing Interest

The authors declare that they have no known competing financial interests or personal relationships that could have appeared to influence the work reported in this paper.

## References

[1] G. Pozzato, A. Allam, S. Onori, Lithium-ion battery aging dataset based on electric vehicle real-driving profiles, Data Br. 41 (2022) 107995, doi:10.1016/j.dib.2022.107995.
[2] K. Moy, S. Onori, Synthetic grid storage duty cycles for second-life lithium-ion battery experiments, SAE Technical Paper Series, SAE International, 2023, doi:10.4271/2023-01-0516.
[3] J. Thakur, C. Martins Leite de Almeida, A.G. Baskar, Electric vehicle batteries for a circular economy: second life batteries as residential stationary storage, J. Clean. Prod. 375 (2022) 134066, doi:10.1016/j.jclepro.2022.134066.

[4] A. Kampker, H.H. Heimes, C. Offermanns, J. Vienenkötter, M. Frank, D. Holz, Identification of challenges for second-life battery systems—A literature review, World Electr. Veh. J. 14 (4) (2023) 80, doi:10.3390/wevj14040080.

[5] San Diego Gas & Electric, 2022. Time of Use (TOU) DR-SES. Available at: https://www.sdge.com/regulatory-filing/2227/time-use-tou.

[6] L.G. Chem, 2018. Product specification, rechargeable lithium-ion battery, model: INR21700 M50T 18.20Wh. Available at: https://www.batteryspace.com/prod-specs/11514.pdf.

[7] M. Steinhardt, E.I. Gillich, A. Rheinfeld, L. Kraft, M. Spielbauer, O. Bohlen, A. Jossen, Low-effort determination of heat capacity and thermal conductivity for cylindrical 18650 and 21700 lithium-ion cells, J. Energy Storage 42 (2021) 103065, doi:10.1016/j.est.2021.103065.

[8] United States Department of Energy, Office of Energy Efficiency & Renewable Energy, 2022. Benchmark Datasets for Buildings.